

## Article

# Simulation of Draught Reduction Performance of Subsoiling with Upcutting Belt Motion Using Discrete Element Method

Peng Gao <sup>1,2</sup>, Jinguang Li <sup>1,2</sup>, Hongyan Qi <sup>1,2</sup>, Xuanting Liu <sup>1,2</sup> and Yunhai Ma <sup>1,2,\*</sup>

<sup>1</sup> The College of Biological and Agricultural Engineering, Jilin University, 5988 Renmin Street, Changchun 130025, China; penggao15@mails.jlu.edu.cn (P.G.); jgli18@mails.jlu.edu.cn (J.L.); qhy18@mails.jlu.edu.cn (H.Q.); xuanting120@mails.jlu.edu.cn (X.L.)

<sup>2</sup> The Key Laboratory of Bionic Engineering, Ministry of Education, Jilin University, 5988 Renmin Street, Changchun 130025, China

\* Correspondence: myh@jlu.edu.cn; Tel.: +86-0431-85095760-413

**Featured Application:** This work proves the feasibility and effectiveness of upcutting belt motion to reduce the draught resistance of subsoilers, which is also a reference and experience for the optimization and modification of other soil-engaging components.

**Abstract:** Conventional subsoiling has the problem of excessive draught resistance, which has long been a major concern. A great reduction in draught is urgently required to make better use of the subsoiling technique with many agronomic benefits. In this study, an attempt was made to test the draught reduction performance of a series of tools with continuous belt motions. Comparative simulations between regular tools and belt tools were carried out using the discrete element method (DEM) to investigate the effects of belt motion on tool force, soil disturbance characteristics, particle velocity distribution, and soil deformation and movement patterns. The results indicated that the belt motion reduced the draught force by 13.18%, 25.21%, 37.98%, and 44.64% for the rake angles of 30°, 45°, 60°, and 75°, respectively, and caused acceptable increases in downward vertical force. The changes in soil disturbance, particle velocity distribution, and soil deformation and movement patterns contributed to the reduction in draught force. Negative effects on soil disturbance were acceptable considering the 13.18% to 44.64% reductions in draught force. The present study suggests that the belt motion has a great application potential for draught reduction in subsoiling. Also, this can serve as a theoretical foundation for future studies.

**Keywords:** subsoiler; discrete element method (DEM); continuous belt; draught force; soil disturbance; particle velocity; specific resistance; soil movement; soil deformation



**Citation:** Gao, P.; Li, J.; Qi, H.; Liu, X.; Ma, Y. Simulation of Draught Reduction Performance of Subsoiling with Upcutting Belt Motion Using Discrete Element Method. *Appl. Sci.* **2024**, *14*, 1313. <https://doi.org/10.3390/app14031313>

Academic Editor: José Miguel Molina Martínez

Received: 19 January 2024  
Revised: 31 January 2024  
Accepted: 2 February 2024  
Published: 5 February 2024



**Copyright:** © 2024 by the authors. Licensee MDPI, Basel, Switzerland. This article is an open access article distributed under the terms and conditions of the Creative Commons Attribution (CC BY) license (<https://creativecommons.org/licenses/by/4.0/>).

## 1. Introduction

The predominant soil–tool interaction of a subsoiler is the cutting of soil by horizontally moving tools (Figure 1). The soil-cutting process often involves a large draught requirement, which is the dominant limitation for determining the extent of its operation [1,2]. To overcome the problem of tillage resistance, soil-engaging components or implements must be designed with high material strength, high structural rigidity, and high tractor power, which causes inconvenience in use and increases production and operating costs [3,4]. For this reason, a method that can significantly reduce the tillage resistance in tillage operations, especially in subsoiling, is urgently needed. This is not only due to cost-saving considerations, but also to the electrification of agricultural machinery, automation, and the inevitable requirements of efficiency and safety [5].

Tillage theories assume that the soil moves upwards in front of the tools along the tool surface (Figure 1b,d) [6,7]. Therefore, existing methods to reduce draught typically focus on reducing friction and adhesion at the soil–tool interface, such as interfacial lubrication [8,9], surfaces made of special materials [10–12], bionic non-smooth surfaces [13–15], and active or

passive vibration [16–18]. However, the assumption is not always valid due to the inherent constraints of interface kinematics [19]. The actual performance of draught reduction is weakened when the surface of the tool is “synchronized” by boundary wedges formed by the failed soil that can barely be displaced relative to the tool [19–22]. A further reduction in draught requires more radical methods. A special form of device that moves horizontally while its surface elements (or components) move upwards appears to have more potential for draught reduction. This approach has proven successful in power-driven active rotary disc tools, where draught can be reduced by over 30% compared to normal discs [4,23,24].

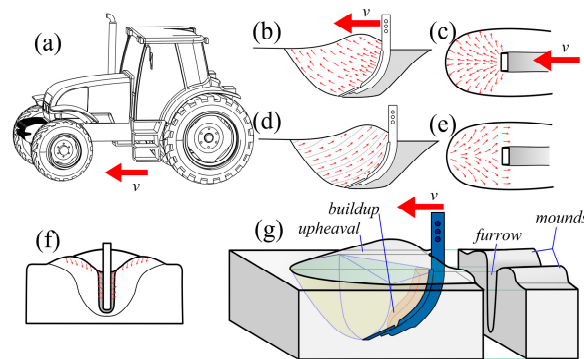


**Figure 1.** Soil–tool interaction system: (a) Tractor traveling at speed  $v$ ; (b–g) Soil disturbance and displacement caused by a horizontally moving subsoiler pulled by the tractor, described using earth coordinate system (ECS) and implement coordinate system (ICS); (b) Elevation view, ECS; (c) Top view, ECS; (d) Elevation view, ICS; (e) Top view, ICS; (f) Rear view; (g) Three-dimensional soil disturbance. (The arrows marked with  $v$  represent the translational motion of the tools in the ECS).

Subsoilers are narrow tools whose working depth is much greater than their width (Figure 1f,g). To achieve the tool motion described above within the subsoiling depth, an upcutting continuous belt, as defined by Mellor [25] and other researchers, with a rake angle of less than  $90^\circ$  can be employed. However, the existing theories on continuous belt machines (or chain trenchers) are not applicable to such an analysis. The reason is that the corresponding kinematic and dynamic analyses do not take into account either the soil failure in front of the tool or the draught reduction performance compared to conventional subsoilers [25–28]. Given the lack of relevant research, the idea of combining a subsoiler with a continuous belt motion needs to be tested.

The discrete element method (DEM) is suitable for testing the idea because it effectively simulates the mechanical behaviors of granular materials [29,30]. The use of DEM avoids the disadvantages of costly and time-consuming experimental methods and assumption-based analytical methods [30–32]. Its applicability and reliability have been extensively verified by simulating the soil–tool interactions of rotary tillers [33], plow discs [34], mold-board plows [35–38], subsoilers [14,18,39,40], and other earthmoving machines.

The objective of this study was to investigate the ability of continuous belt motions to reduce the draught requirement of a subsoiler. An attempt was made to test the draught reduction performance of a series of narrow tools with continuous belt motions. Comparative DEM simulations between regular tools and belt tools were carried out to investigate the difference in tool force. Soil disturbance characteristics, particle velocity distribution, and deformation and soil movement patterns were analyzed to explain the difference in tool force. This study provides scientific guidance and a theoretical basis for the application of belt motions in subsoiling machinery and other earth-moving machinery.

## 2. Materials and Methods

### 2.1. Tools and Soil Bin Modelling

A commercial software, EDEM 2018 (DEM Solutions, Ltd., Edinburgh, UK) was used to simulate the soil–tool interaction. A series of simple narrow tine models including

regular tools and tools with belt motions (referred to in the future simply as belt tools) were developed in the simulation (Figure 2). The use of the simple narrow tines was based on the consensus that a clear understanding of the soil–tool interactions of the simple narrow tines would lead to further understanding of the more complex soil–tool interactions [6]. The tine models were 30 mm in width, 260 mm in height, and 5 mm in thickness. The rake angles of the tines were set to 30°, 45°, 60°, and 75°. The aim of the simulation was to investigate the effects of belt motion on draught reduction performance at various rake angles.

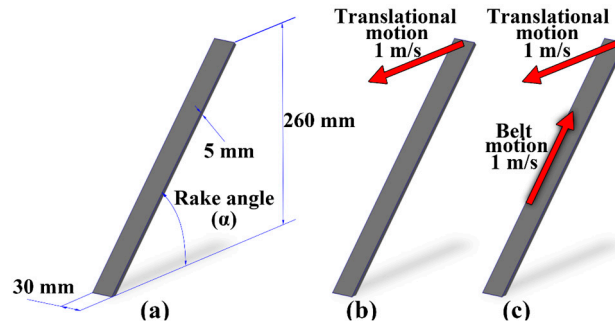


**Figure 2.** Tool model developed in the simulation: (a) Simple tine model (rake angle  $\alpha = 30^\circ, 45^\circ, 60^\circ,$  and  $75^\circ$ ); (b) Regular tool; (c) Belt tool.

A soil bin model that was 1100 mm in length, 400 mm in width, and 500 mm in height was used to contain the soil. The width and depth were large enough for the tool models to disturb the soil based on simulation experiences. On the other hand, the length was enough for the tool models to cut the soil in a steady state [6].

The tool model was positioned at 150 mm depth of cutting in the plane of symmetry of the soil bin. A 1 m/s positive translational constraint along the  $x$ -axis of the soil bin was set for each of the tools to achieve a constant speed of cutting. For each of the belt tools, an additional conveyor belt constraint of 1 m/s upward along the soil-engaging face (front surface) of the tool was set to achieve the belt motion. The following interpretation was made based on the coordinate system in the simulation to avoid confusion: the  $x$ -axis was the longitudinal direction, which was the travel direction of the tool; the  $y$ -axis was the lateral or transverse direction of the tool; and the  $z$ -axis was the vertical direction (Figure 3a).

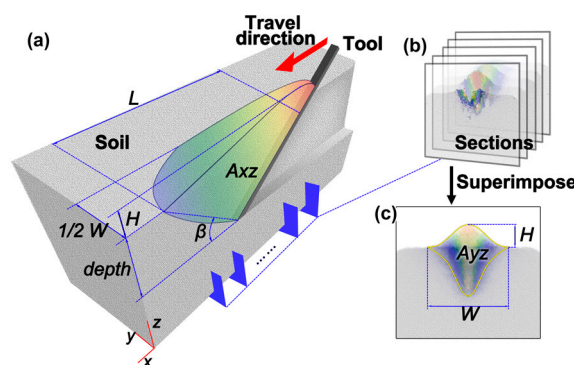


**Figure 3.** Schematic diagram of soil disturbance: (a) Three-dimensional soil disturbance and longitudinal section; (b) Images of transverse sections; (c) Superimposed image.

### 2.2. Parameters Used in EDEM

The properties related to soil–tool interactions were defined by particle models, material parameters, and contact models in EDEM software. The parameters used in the modeling were selected from published data to ensure the reliability of comparative simulations. It has been shown that a reasonable simulation can still be performed when a larger particle size than reality is used [30]. As a result, the efficiency of the simulation can

be greatly improved especially for a limited computational power. Therefore, spherical particles with a radius of 3 mm were used as the particle model. The properties of materials were defined by density ( $\rho$ ), Poisson's ratio ( $\gamma$ ), and shear modulus ( $G$ ). The properties of a Hertz–Mindlin non-slip contact model were defined by the coefficient of restitution, static friction, and rolling friction. The values of the parameters referred to the settings of Tong's work [39] (Table 1). The rules for the interaction between a tool made of 65 Mn steel and a typical black loamy soil (clay 9.6%, silt 44.0%, and sand 46.4%) commonly found in the farmlands in northeastern China were defined by the parameter combination above.

A Rayleigh time step of  $5.13 \times 10^{-5}$  s was generated. A fixed time step was set to  $2.57 \times 10^{-6}$  s, which was 5% of the Rayleigh time step. The total simulation time was 3 s.

**Table 1.** Particle, material, and interaction parameters used in EDEM.

Category	Parameter	Value
Particle	Radius/mm	3
Material	Density of particle/(kg·m <sup>-3</sup> )	2620
	Poisson's ratio of soil	0.33
	Shear modulus of soil/Pa	$1.02 \times 10^8$
	Density of steel/(kg·m <sup>-3</sup> )	7850
	Poisson's ratio of steel	0.3
	Shear modulus of steel/MPa	$7.9 \times 10^{10}$
Interaction	Coefficient of restitution, soil-soil	0.53
	Coefficient of static friction, soil-soil	0.53
	Coefficient of rolling friction, soil-soil	0.42
	Coefficient of restitution, soil-steel	0.27
	Coefficient of static friction, soil-steel	0.54
	Coefficient of restitution, soil-steel	0.28

### 2.3. Tool Force and Soil Disturbance Characteristics Obtaining in EDEM

Much importance is attached to force and soil disturbance characteristics in assessing the tool performance. The tool force and the range of disturbance increase as the tool advances until the cutting is in a steady state. Then, they fluctuate within relatively constant ranges due to the periodic nature of soil–tool interaction in soil cutting [6,39]. A failure boundary completely develops at the moment when the tool force is minimal [41]. The range of disturbance at that moment is typical. Therefore, the tool force in the steady state and the soil disturbance at the moment of minimal tool force were investigated in the Analyst module in EDEM.

The average draught force ( $F_x$ ) and average vertical force ( $F_z$ ) in the steady state were obtained. The particles were displayed in gradient colors based on their velocity (0–1 m/s) so as to distinguish the disturbed particles from those undisturbed. The cross-sections perpendicular to the  $x$ -axis were selected at intervals of 50 mm within the range of disturbance (Figure 3b). The images of transverse disturbance were obtained by superimposing the cross-sections using the “stack” function in ImageJ (v.1.51J) software (National Institutes of Health, USA) (Figure 3c). The images of longitudinal disturbance in the plane of symmetry were also obtained.

The disturbance was quantified using ImageJ software. The profiles of the disturbance were mapped by identifying the undisturbed particles. The values of disturbance width ( $W$ ), upheaval height ( $H$ ), and the area of transverse disturbance ( $A_{yz}$ ) were obtained by measuring the images of the transverse disturbance. Forward rupture distance ( $L$ ), rupture angle ( $\beta$ ), and the area of longitudinal disturbance ( $A_{xz}$ ) were obtained by measuring the images of the longitudinal disturbance. These items are graphically illustrated in Figure 3. The measured values were transferred into actual values based on the scale of the image.

### 2.4. Particle Velocity Distribution Obtaining in EDEM

Tool forces and soil disturbance reflect the difficulty with which the tool causes the soil to move. It can be further characterized by the velocity distribution of the particles in the longitudinal section corresponding to the minimal tool force. Therefore, the particle velocity distribution was analyzed in order to explain the mechanism of the change in tool force.

The magnitude distribution of particle velocity was analyzed conveniently using the images of longitudinal disturbance since the particles were already displayed in gradient colors based on velocity.

The direction distribution of particle velocity was analyzed in an indirect way. A rectangular area of 480 mm × 320 mm centered on the zone of disturbance was divided into 24 × 16 grid cells using the “grid bin group” tool. Then, the grid cells were displayed in gradient colors based on the average direction (an angle with the *x*-axis) of the velocity vectors in each grid cell. The direction distribution of particle velocity was analyzed based on the average directions.

### 2.5. Deformation and Movement Patterns Obtaining in EDEM

Soil deforms and moves as the tool advances [6,42]. The patterns of deformation and movement change as the rake angle and the kinematic condition of the interface change. Therefore, the soil deformation and movement in the longitudinal section were analyzed in detail in order to further explain the mechanism of the change in tool force.

A square slice (100 mm × 100 mm) within the longitudinal section was displayed in red at the very initial moment of soil cutting. The images of the slice during the process of cutting were captured at time intervals of 0.1 s. Then, the images were superimposed using ImageJ. The soil deformation and movement were illustrated by the red square slice whose subsequent positions and shapes corresponded to the moving tool. The analysis was conducted qualitatively due to the irregularity of the shape of the slice at the subsequent moments.

## 3. Results and Discussion

### 3.1. Tool Force

The simulation showed the effects of rake angle and belt motion on tool force (Figure 4). The average draught force (*F<sub>x</sub>*) increased as the rake angle increased (Figure 4a). The minimal values of *F<sub>x</sub>* for the regular tools and the belt tools were 126.7 N and 110 N, respectively, at the rake angle of 30°. Then, the belt tools showed a lower increase rate of *F<sub>x</sub>* than the regular tools. The *F<sub>x</sub>* values for the belt tools were 13.18%, 25.21%, 37.98%, and 44.64% lower than those for the regular tools at the rake angles of 30°, 45°, 60°, and 75°, respectively. These results indicate a significant reduction in draught force as influenced by the belt motion, and the reduction is higher when the rake angle is larger.

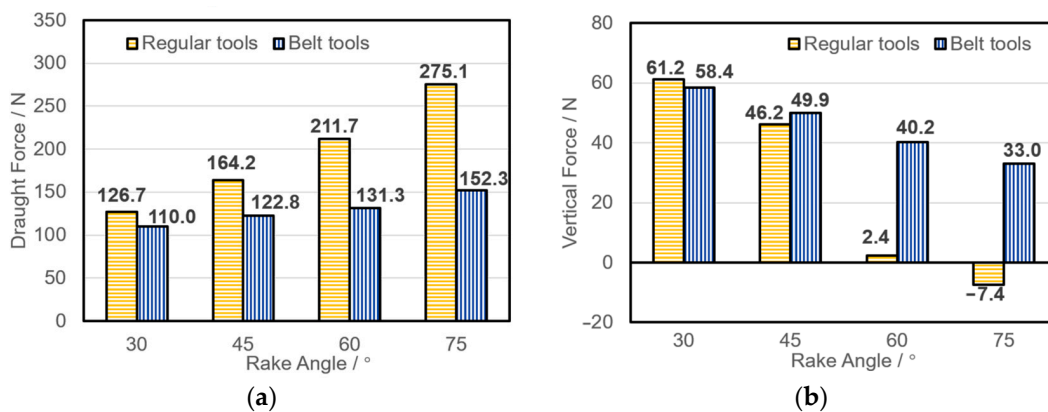


**Figure 4.** Tool force: (a) Average draught force; (b) Average vertical force (negative vertical force is in an upward direction).

The simulation also showed that the average vertical force ( $F_z$ ) had an opposite trend as the rake angle increased (Figure 4b). The maximal values of  $F_z$  were 61.2 N and 58.4 N for the regular tools and belt tools, respectively, at the rake angle of 30°. Then the belt tools showed a lower decrease rate of  $F_z$  than the regular tools. The  $F_z$  values for the belt tools were 8.01% and 1575.0% higher than those for the regular tools at the rake angles of 45° and 60°, respectively. The  $F_z$  for the regular tools at the rake angle of 75° had a reversed direction upwards, but the  $F_z$  for the belt tools remained downward. These results indicate that the belt motion tends to increase the downward vertical force when the rake angle is large, but the effect is dependent on the rake angle.

The force change is partly attributed to the change in the patterns of soil deformation and movement. The increase in rake angle turns the patterns from “cutting” into “pushing” [35,40,43]. This transition means the direction in which the tool applies forces to the soil and the direction in which these forces cause the soil to move have changed [1]. Consequently, the inevitable effects change the equilibrium of the soil, which increases the tool force. However, the belt motion changes the range of disturbance, the particle velocity distribution, and the soil deformation and movement patterns. All these changes are conducive to reducing the draught force. They are discussed in the following sections.

On the other hand, although the downward vertical forces were increased by the belt motion, they were no larger than those for the regular tools with a rake angle of 30°. A larger vertical force is harmful due to the negative effects of excessive downward penetration and soil compaction [39]. However, a vertical force within a reasonable range is acceptable, and can be counterbalanced by soil reactions. Therefore, concerns are mainly focused on the reasons for the change in draught force in the following discussions.

### 3.2. Soil Disturbance Characteristics

#### 3.2.1. Transverse Disturbance

The simulation showed the effects of rake angle and motion on transverse disturbance (Figure 5). The transverse disturbance for the regular tools and the belt tools at the four rake angles showed a similarity in shape, which was the combination of a soil upheaval above the original soil surface and an inverted triangular zone below the surface (Figure 5).

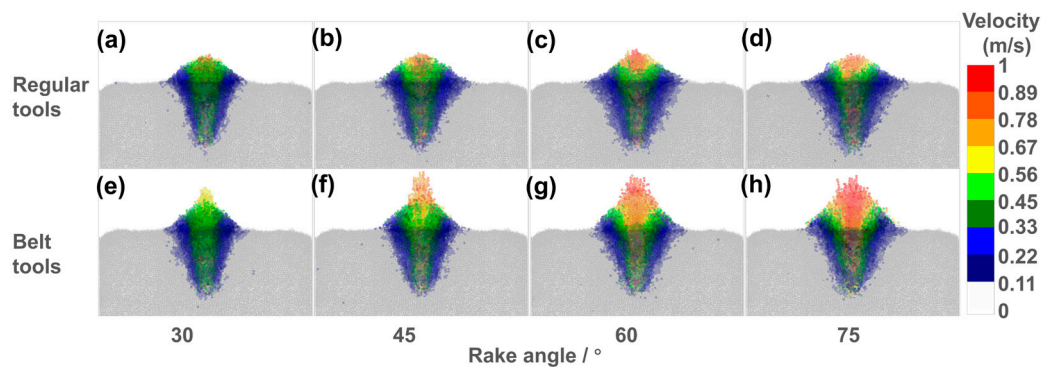


**Figure 5.** Transverse disturbance: (a–d) Regular tools; (e–h) Belt tools (rake angle  $\alpha = 30^\circ, 45^\circ, 60^\circ, 75^\circ$ ).

The area of transverse disturbance ( $A_{yz}$ ) increased as the rake angle increased (Figure 6). However, the  $A_{yz}$  values for the belt tools were higher than those for the regular tools. This was related to the changes in disturbance width ( $W$ ) and upheaval height ( $H$ ) (Figure 7). Although the  $W$  values for the belt tools were slightly lower, the  $H$  values for the belt tools were higher than those for the regular tools at the four rake angles. Therefore, the higher values of  $A_{yz}$  for the belt tools were mainly attributed to the increased upheaval height ( $H$ ).

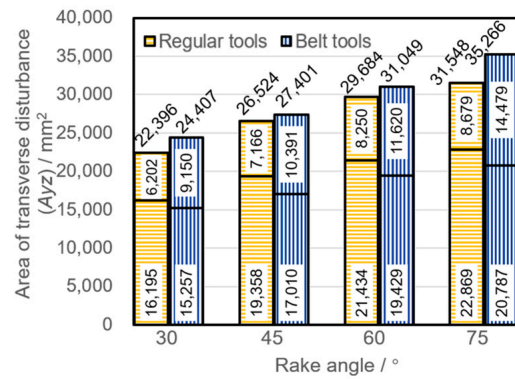


**Figure 6.** Area of transverse disturbance ( $A_{yz}$ ). (The upper half of each bar represents the area of soil disturbance above the initial ground surface, while the lower half represents the area of soil disturbance below the ground surface).

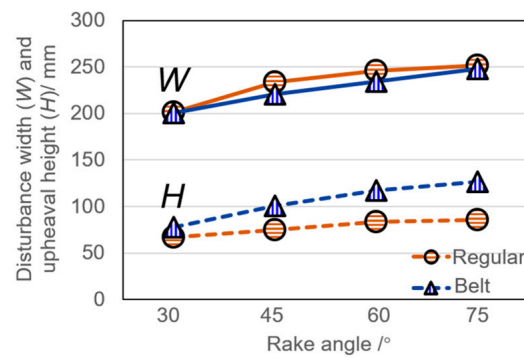


**Figure 7.** Disturbance width ( $W$ ) and Upheaval height ( $H$ ).

The areas of the underground disturbance for the two types of tools were similar because of the identical depth of cutting and the similarity in disturbance width ( $W$ ); thus, the overall effect of the belt motion was acceptable considering the specific resistance of subsoiling, which is the ratio of draught force to the area of underground disturbance as shown in Equation (1) [43].

$$K_f = F_x / A_f, \tag{1}$$

where  $K_f$  denotes the specific resistance ( $\text{kN}/\text{m}^2$ ) and  $A_f$  denotes the area of underground disturbance.

The specific resistance ( $K_f$ ) for the belt tools was lower than that for the regular tools (Figure 8). The  $K_f$  value increased from 7.82 to 12.03 for the regular tools, while remained about 7 for the belt tools as the rake angle increased.

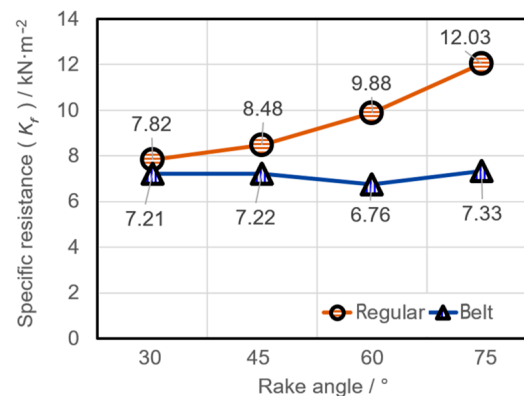


**Figure 8.** Specific resistance ( $K_f$ ). (Random disturbance results in slightly fluctuating  $K_f$  values).

The specific resistance of subsoiling is an indicator to assess the performance and efficiency of subsoiling, which reflects the draught force requirement of a subsoiler disturbing a given cross-sectional area. A lower specific resistance indicates a better subsoiling efficiency [39]. The above results indicate that the belt motion increases the subsoiling efficiency by reducing the specific resistance.

### 3.2.2. Longitudinal Disturbance

The simulation showed the effects of rake angle and belt motion on longitudinal disturbance (Figure 9). The area of longitudinal disturbance ( $A_{xz}$ ) decreased as the rake angle increased (Figure 10). Meanwhile, the failure boundary became curvier gradually (Figure 9). The  $A_{xz}$  values for the regular tools and the belt tools were maximal at the rake angles of  $30^\circ$ , then decreased at different rates as the rake angle increased. The  $A_{xz}$  values for the belt tools were 3.54%, 4.46%, and 6.98% lower than those for the regular tools at the rake angles of  $45^\circ$ ,  $60^\circ$  and  $75^\circ$ , respectively (Figure 10). Additionally, the failure boundaries were straighter for the belt tools than those for the regular tools (Figure 9). These results indicate that the belt motion reduces the area of longitudinal disturbance and changes its shape especially when the rake angle is larger.

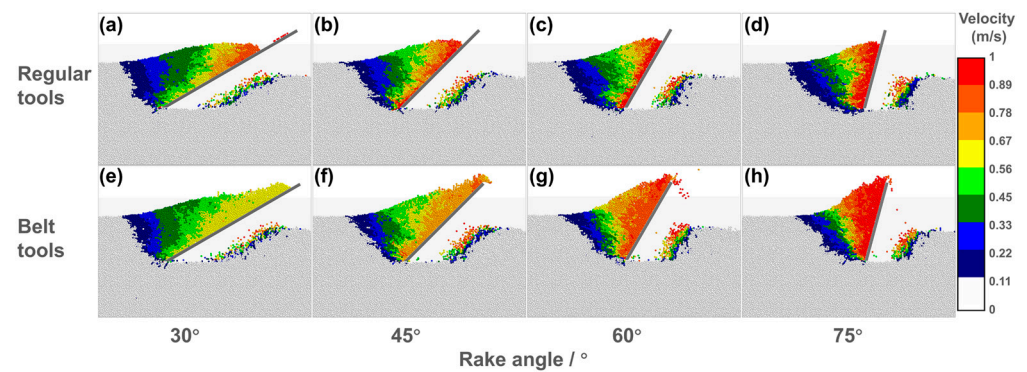


**Figure 9.** Longitudinal disturbance and particle velocity distribution: (a–d) Regular tools; (e–h) Belt tools (rake angle  $\alpha = 30^\circ, 45^\circ, 60^\circ, 75^\circ$ ).

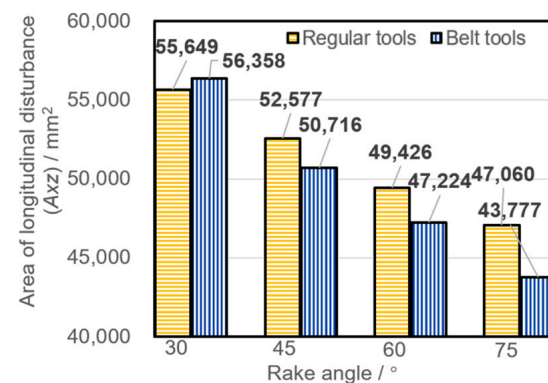


**Figure 10.** Area of longitudinal disturbance ( $A_{xz}$ ).

The decrease in the area of longitudinal disturbance ( $A_{xz}$ ) caused by the belt motion was related to the decreases in rupture angle ( $\beta$ ) and forward rupture distance ( $L$ ) (Figures 11 and 12). The  $\beta$  and  $L$  values for the belt tools were about  $1\text{--}5^\circ$  and about 7% lower than those for the regular tools, respectively. Therefore, the changes in these two parameters as well as the increase in upheaval height ( $H$ ) contributed to the changes in the area of longitudinal disturbance ( $A_{xz}$ ).

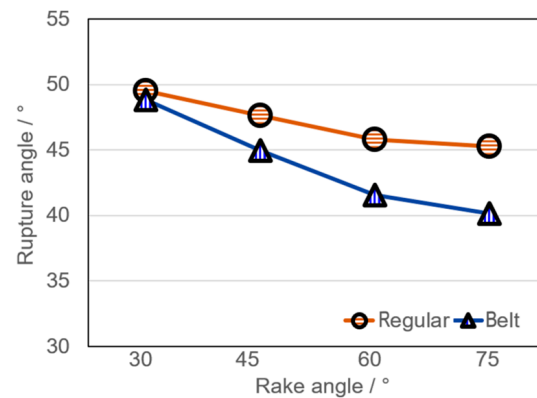


**Figure 11.** Angle of Rupture ( $\beta$ ).

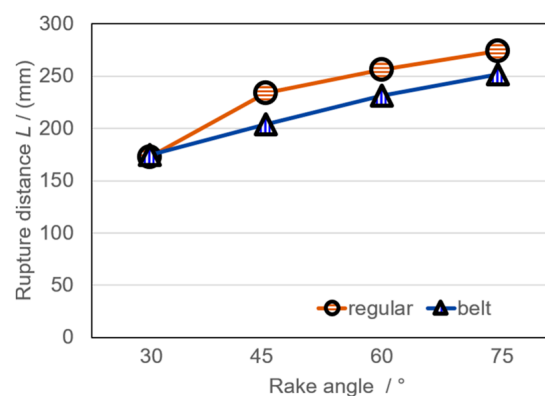


**Figure 12.** Rupture distance (L).

In general, small rake angles lead to relatively straighter failure boundaries, larger rupture angles, and smaller rupture distances, whereas large rake angles have the opposite trends [41]. These are the differences between “cutting” and “pushing” [35]. The belt motion tends to reduce the “pushing”, though its effect is also different from the “cutting”. This means the direction in which the tool applies forces to the soil and the direction in which these forces cause the soil to move has changed [1]. The changes in longitudinal disturbance are closely related to the change in tool force. The draught component of the tool force decreases for the reduced “pushing”. The tool force decreases since less soil interacts with the tool, which is reflected in the reductions in the area of longitudinal disturbance and rupture distance [39]. Therefore, the comprehensive effect of belt motion on longitudinal disturbance is one of the reasons for the reduction in tool force.

### 3.3. Particle Velocity Distribution

The simulation showed the effects of rake angle and belt motion on particle velocity distribution (9). The magnitude distribution of particle velocity changed as the rake angle increased (Figures 9a–d and 9e–h, respectively). The particles with the highest velocities (close to 1 m/s, red) gradually occupied the entire tool face, and gradually replaced the particles with medium velocities (0.33 to 0.78 m/s, yellow to green). While the particles with the lowest velocities (close to 0 m/s, blue) barely changed. However, there were differences in the magnitude distribution of particle velocity between the belt tools and the regular tools at the same rake angles. The belt tools had more low-velocity particles (yellow to green) in their vicinity than the regular tools when the rake angles were 30° and 45° (Figures 9a,b and 9e,f, respectively), but more high-velocity particles (close to 1 m/s, red) in the cases of the rake angles 60° and 75° (Figures 9c,d and 9g,h, respectively).

The particle velocity showed a correlation between its magnitude and direction distributions (Figure 13). The particle velocity vectors mostly pointed obliquely at the soil surface

in front of the tool. The average vector direction in the grid cells ranged from 0 to 50° (yellow to green cells). There were more particles moving in lower directions as the rake angle increased (Figures 13a–d and 13e–h, respectively). The particles moving in average directions lower than 30° (green) gradually replaced those higher than 30° (yellow) and gradually occupied the entire tool face. However, the belt tools had more particles moving in average directions higher than 30° (yellow) than the regular tools (Figures 13a,e, 13b,f, 13c,g and 13d,h, respectively). The results show that the belt motion leads to an increase in the direction of particle velocity.

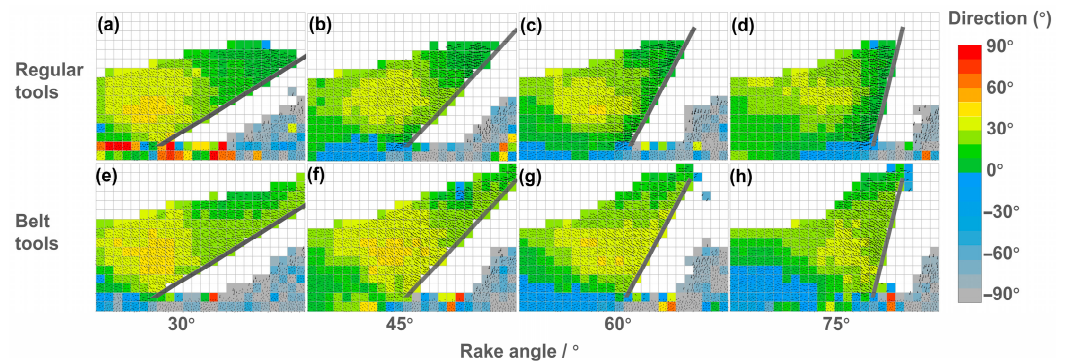


**Figure 13.** Direction distribution of particle velocity: (a–d) Regular tools; (e–h) Belt tools (rake angle  $\alpha = 30^\circ, 45^\circ, 60^\circ, 75^\circ$ ). (Notes: The particles in the red to green grid cells mostly move upwards and forwards; the particles in blue to gray grid cells mostly move downwards and forwards).

The above results indicate that the distribution of particle velocity in the longitudinal section is affected by the rake angle and the belt motion. A larger rake angle results in more forward particle movement, while the belt motion makes more particles move upwards. A typical soil particle velocity in the vicinity of the tool face usually has a large horizontal component that is close to the operating speed of the tool. This makes the particles move slowly relative to the tool face. Then, a soil buildup develops on the tool face [19]. The buildup is considered to be negative to subsoiling. It reduces the rate of soil replacement in the disturbance zone, and changes the tool shape. Also, it may intensify the soil compression in the disturbance zone and increase the friction on the tool surface [24]. These all result in an increase in draught force. However, the belt motion leads to more soil particles in deep layers escaping to the free surface as well as the soil in the disturbance zone being rapidly replaced by subsequent soil, which reduces the soil compression in the disturbance zone. This is another reason for the reduction in draught force.

### 3.4. Soil Deformation and Movement Patterns

The simulation showed the effects of rake angle and belt motion on soil deformation and movement patterns in the longitudinal section (Figure 14). The square slice experienced a shortening in width and a lengthening in height and gradually became elongated and irregular as the tool advanced. In the meantime, the main part of the slice moved forward and upwards as a whole from its initial position and eventually over the soil surface.

The soil deformation and movement intensified as the rake angle increased (Figures 14a–d and 14e–h, respectively). The slice was slenderer and moved further as the rake angle increased from 30° to 45°, and 60° and 75°. However, the belt tools made the slice wider and shorter, and moved the slice higher but closer than the regular tools at the same rake angles.

In general, the original structure of soil is destructed and loosened by an incipient soil failure. However, the soil is subjected to an intensified “pushing” as the rake angle increases. The loosened soil experiences secondary compactions by the subsequent movements of the tool especially for the larger rake angles [24]. The unnecessary secondary compaction is partly responsible for the high draught force. The belt motion reduces the compression by

transporting the soil from deep layers to the free surface, and then the unnecessary draught force consequently decreases.

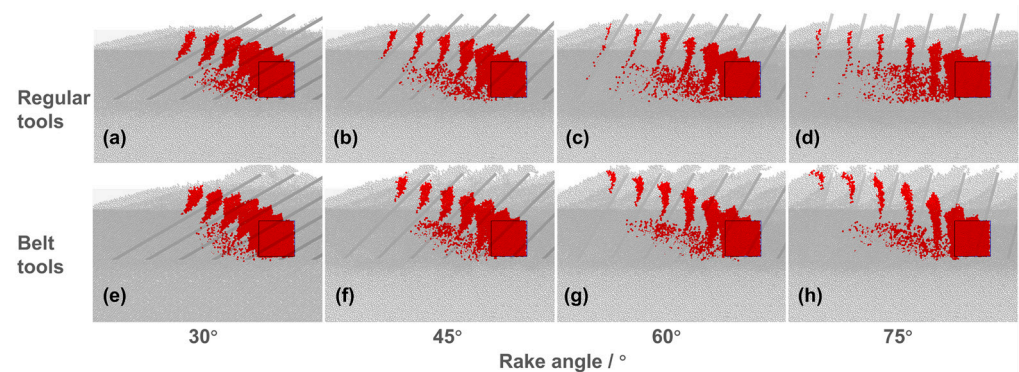


**Figure 14.** Soil deformation and movement patterns: (a–d) Regular tools; (e–h) Belt tools (rake angle  $\alpha = 30^\circ, 45^\circ, 60^\circ, 75^\circ$ ).

#### 4. Discussion

The objective of this study was to evaluate the draught reduction performance of subsoilers with belt motions. It is clear that the belt motion exhibits a significant draught reduction performance within the operating conditions set in the simulation referring to the analysis in Section 3. For the regular tools, the draught force increases as the rake angle increases, and this trend has been widely observed [7,41,44,45]. In the case of belt tools, the draught force can be reduced by 13.18% to 44.64% with rake angles ranging from 30° to 75°. The advancement of tools applied forces on soil particles and forced them to move. The actual direction in which the surface elements of the belt tools move points obliquely at the free surface in front of the tool [25]. Such a tool motion is responsible for the reduction in draught force. The vertical components of the resultant force applied to the soil are reasonably larger as the rake angle increases. For this reason, the maximum draught reduction ratio was obtained at the rake angle of 75°. An analogous draught reduction performance could be found in other types of belt machines and power-driven discs, although either the cutting mechanism or the operating mode may be partially different [4,23–28]. As described in Section 3.1, these results can be explained by the influence of belt motion on soil disturbance characteristics, soil particle velocity distribution, and soil deformation and movement patterns.

First, the belt motion changes the range of soil disturbance. The longitudinal failure boundary is the path of the farthest positions where the tool causes disturbance [46]. The soil failure occurs in a linear manner or logarithmic spiral manner of the minimum resistance path. Under the influence of belt motions, the change in the direction of external friction causes the principal stress axis to rotate [20], resulting in an associated rotation of the failure boundary. The results in Section 3.2 indicate that the forward failure distance  $l$  decreases accordingly, the rupture angle  $\beta$  increases, and this inevitably leads to a relative reduction in area of longitudinal disturbance. Since the draught force is a function of the rupture angle  $\beta$  [24], the reduced area of disturbance indicates a decrease in the working volume of the soil, corresponding to a lower draught force. This is consistent with results obtained on power-driven discs performing similar soil operations [24].

Second, the belt motion changes particle velocity distribution. In Section 3.3, the magnitude and direction of particle velocity near the tool surface are close to the velocity of the traveling tool, which is consistent with the velocity field obtained by DEM simulations [29,47], finite element simulations [48,49], and glass-sided soil bin experiments [20,50]. Under certain initial conditions, soil particles continuously accumulate on the tool surface, forming a boundary wedge that moves synchronously with the tool [19,22]. The boundary wedge changes the macroscopic shape of the tool, causing soil to accumulate in front of the tool, making it difficult to replace soil smoothly and exerting a compressive force on the

next soil, which leads to an increase in draught force [24,29,40]. The results in Section 3.3 indicate that the vertical component of particle velocity increases as the belt motion worked, and thus changed the direction of the force applied to soil particles. This adds “lifting” based on “pushing” [35,40,45]. On the other hand, the soil particles on the tool surface have a greater tendency to move relative to the tool surface, which relieves the accumulation. The particle velocity changed from a nearly horizontal direction into an obliquely upward direction, resulting in a decrease in draught force. As another result, the accumulated soil upheaval and the soil mounds on both sides of the furrow may become larger. However, they partially fall into the furrow after the pass of the subsoiler, or these mounds are removed by subsequent surface leveling operations. The use of power-driven disc tools has also shown that soil transportation (displacement) can reduce draught force [24].

Finally, the belt motion changes soil movement and deformation patterns. The tool advance causes soil compression, and the draught force increases [6,42]. The soil deforms and moves continuously until the soil is no longer under the influence of the tool [6,42,51,52]. The failing soil in compression develops high draught forces and is inefficient in energy use per unit volume of soil disturbed, despite the fact that most modern passive subsoiling tools do so. This is a fundamental flaw in current design concepts for soil-loosening tools [21,53,54]. The results in Section 3.4 show that the belt motion increases upward soil movement, reduces soil compaction, and thus reduces draught force by “lifting”. The results are in agreement with the analysis of Spoor and Fry [55] that no compaction will occur providing the vertical component of movement is sufficiently great. This occurs when the upward movement is unrestricted leading to a state of lower compressive stress in the soil. This is also consistent with the viewpoint of critical state soil mechanics that the only soil loosening process is shearing at relatively low compressive stresses [21,56]. On the other hand, the belt motion may induce some tensile stress in the unsupported upper soil in front of the tool [54]. It is common knowledge that the inherent tensile strength of soils is several orders of magnitude lower than its shear strength induced by compressive stresses. Therefore, such a condition leads to easier soil failure and lower draught force [54].

Draught reduction has many beneficial effects. High tractor power is usually required to overcome large draught resistance, while forced operation would result in deformation and wear of the tool, as well as incorrect working conditions, lower working efficiency, and unacceptable tillage quality. However, by reducing the draught resistance, it is possible to use lighter tractors with less traction power, and higher speed, and avoid various problems above caused by excessive resistance. These further helped to reduce the manufacturing cost of the tractor and implement [24].

However, the risk of applying the above principle to subsoilers is a possible controversy in practical application. First, moving parts (e.g., chains) in contact with soil may cause mechanical failure, and the complex structure may also increase the manufacturing cost. Second, incorrect belt width and speed may transport more subsoil resulting in oversized furrows, which is unacceptable. Third, additional energy is required to drive the belt, which makes the energy consumption performance uncertain. This requires further study. Despite these controversies, this should not prevent the use of the principle. These controversial negative effects can be avoided by careful mechanical design. Considering the successful application of belt-like devices with different structures and engineering purposes, such as chain trenchers, potato or onion diggers, belt soil throwers, coal saws, etc., subsoiling with an upcutting belt motion would be feasible. The excellent draught reduction capability solves the most pressing problem of large draught requirements in subsoiling or other types of tillage, which deserves more attention. This technology has wide application prospects.

It should be noted that this study is not exhaustive due to space limitations. First, only one soil particle diameter was used in the simulation, which obviously cannot represent the widespread changes in soil type and condition in nature. However, the simulation clearly showed the draught reduction performance of the belt tools under the same given soil conditions. Similar trends in the draught reduction performance of belt tools would

be expected if different soil conditions were used. This is because the characteristic of large soil deformation due to tillage tool interaction can be viewed as soil flow around the tillage tool (Figure 1d,e). Different patterns of soil failure may be similar in the “macroscale” nature of soil movement [47,51]. Nevertheless, future studies need to carefully investigate the draught reduction performance of belt motions under different soil conditions. Furthermore, different belt speeds should be investigated in addition to the typical belt speed of 1 m/s used in the simulation. This is because faster belt speeds are likely to remove more soil, which may further reduce the draught force. Therefore, more research on the effect of belt speed on draught force is needed. The third issue is that the external power driving the belt motion requires additional power consumption, which is also closely related to the belt speed. Therefore, further research should include the optimal belt speed to achieve the maximum draught reduction effect with the minimum power consumption. These are subjects worthy of further research. However, the significance of this article is that it confirms the idea that belt motions can significantly reduce the draught force, as well as the reasons for the reduction. The actual draught reduction performance of the belt tools can be further verified by soil bin and field studies.

## 5. Conclusions

In this study, the draught reduction performance of the tool with upcutting continuous belt motion was investigated through comparative DEM simulations. The results showed that the belt motion can significantly reduce the draught resistance, and the reduction can be explained by the changes in soil disturbance characteristics, particle velocity distribution, and soil deformation and movement patterns. The main findings from the results were summarized as follows:

- (1) The belt motion significantly reduces the draught force by 13.18–44.64%, but increases the downward vertical force within a reasonable range.
- (2) The belt motion increases the area of transverse disturbance, but reduces the area of longitudinal disturbance. The belt motion also changes the shapes of soil disturbances.
- (3) The belt motion causes more soil particles to move upward at a higher speed relative to the tool preventing the development of soil buildup.
- (4) The belt motion relieves soil compression and transports the soil upwards by changing the soil deformation and movement patterns.
- (5) The changes in soil disturbance, particle velocity distribution, and soil deformation and movement patterns contribute to the reduction in draught force.

This study indicates that the belt motion has great potential in reducing the draught force of subsoiling. The study also provides detailed scientific guidance and a theoretical basis for the future design of low-draught subsoilers and other earth-moving machines based on the upcutting continuous belt.

**Author Contributions:** Conceptualization, P.G. and Y.M.; Data curation, P.G. and X.L.; Formal analysis, P.G. and J.L.; Funding acquisition, Y.M.; Investigation, P.G. and J.L.; Methodology, P.G. and J.L.; Project administration, Y.M.; Resources, Y.M.; Software, P.G. and X.L.; Supervision, Y.M.; Validation, J.L., H.Q. and X.L.; Visualization, P.G. and X.L.; Writing—original draft, P.G., J.L. and H.Q.; Writing—review and editing, Y.M. All authors have read and agreed to the published version of the manuscript.

**Funding:** This research was funded by the National Natural Science Foundation of China (grant number 52275288); National Key Research and Development Program of China (grant number 2023YFD2000903); the Jilin Province Science and Technology Development Plan Item (grant number 20210202021NC).

**Institutional Review Board Statement:** Not applicable.

**Informed Consent Statement:** Not applicable.

**Data Availability Statement:** The raw data supporting the conclusions of this article will be made available by the authors on request.

**Acknowledgments:** The authors are grateful to the editors' immediate processing, and the anonymous reviewers for their valuable suggestions.

**Conflicts of Interest:** The authors declare no conflicts of interest.

## References

- Gill, W.R.; Vandenberg, G.E. *Soil Dynamics in Tillage and Traction, Agricultural Handbook No.316*; Agricultural Research Service US, Department of Agriculture: Washington, DC, USA, 1967; pp. 230–231.
- Manuwa, S. Performance evaluation of tillage tines operating under different depths in a sandy clay loam soil. *Soil Tillage Res.* **2009**, *103*, 399–405. [[CrossRef](#)]
- Salokhe, V.; Quang, N.B. Dynamics of a powered disk in clay soil. *J. Terramechanics* **1995**, *32*, 231–244. [[CrossRef](#)]
- Hann, M.; Giessibl, J. Force Measurements on Driven Discs. *J. Agric. Eng. Res.* **1998**, *69*, 149–157. [[CrossRef](#)]
- Hemami, A. Motion trajectory study in the scooping operation of an LHD-loader. *IEEE Trans. Ind. Appl.* **1994**, *30*, 1333–1338. [[CrossRef](#)]
- Makanga, J.; Salokhe, V.; Gee-Clough, D. Effects of tine rake angle and aspect ratio on soil reactions in dry loam soil. *J. Terramechanics* **1997**, *34*, 235–250. [[CrossRef](#)]
- Godwin, R.; Spoor, G.; Leeds-Harrison, P. An Experimental Investigation into the Force Mechanics and Resulting Soil Disturbance of Mole Ploughs. *J. Agric. Res.* **1981**, *26*, 477–497. [[CrossRef](#)]
- Araya, K. Soil Failure Caused by Subsoilers with Pressurized Water Injection. *J. Agric. Eng. Res.* **1994**, *58*, 279–287. [[CrossRef](#)]
- Larson, D.L.; Clyma, H.E. Electro-osmosis effectiveness in reducing tillage draft force and energy requirements. *Trans. ASAE* **1995**, *38*, 1281–1288. [[CrossRef](#)]
- Salokhe, V.; Gee-Clough, D. Technology showcase applications of enamel coating in agriculture. *J. Terramechanics* **1989**, *26*, 275–286. [[CrossRef](#)]
- Tong, J.; Lu, X.; Chen, Y.; Ren, L.; Chen, B. Soil Adhesion and Abrasive wear of PTFE-Matrix Composites. *Trans. Csaе* **1990**, *6*, 13–19. (In Chinese)
- Tong, J.; Ren, L.; Chen, B.; Qaisrani, A. Characteristics of adhesion between soil and solid surfaces. *J. Terramechanics* **1994**, *31*, 93–105. [[CrossRef](#)]
- Ren, L.; Han, Z.; Li, J.; Tong, J. Effects of non-smooth characteristics on bionic bulldozer blades in resistance reduction against soil. *J. Terramechanics* **2002**, *39*, 221–230. [[CrossRef](#)]
- Sun, J.; Wang, Y.; Ma, Y.; Tong, J.; Zhang, Z. DEM simulation of bionic subsoilers (tillage depth > 40 cm) with drag reduction and lower soil disturbance characteristics. *Adv. Eng. Softw.* **2018**, *119*, 30–37. [[CrossRef](#)]
- Tong, J.; Wu, B.; Song, Z.; Gao, Z.; Sun, J.; Ma, Y.; Zhuang, J. Research on the drag reduction mechanism of antlion (*Myrmeleon sagax*) larvae nonsmooth structural surface. *Microsc. Res. Tech.* **2020**, *83*, 338–344. [[CrossRef](#)]
- Bandalan, E.; Salokhe, V.; Gupta, C.; Niyamapa, T. Performance of an oscillating subsoiler in breaking a hardpan. *J. Terramechanics* **1999**, *36*, 117–125. [[CrossRef](#)]
- Niyamapa, T.; Salokhe, V. Force and Pressure Distribution under Vibratory Tillage tool. *J. Terramechanics* **2000**, *37*, 139–150. [[CrossRef](#)]
- Wang, Y.; Zhang, D.; Yang, L.; Cui, T.; Jing, H.; Zhong, X. Modeling the Interaction of Soil and a Vibrating Subsoiler Using the Discrete Element Method. *Comput. Electron. Agric.* **2020**, *174*, 105518. [[CrossRef](#)]
- Hettiaratchi, D.R.P.; Reece, A.R. Boundary Wedges in two-dimensional passive soil failure. *Geotechnique* **1975**, *25*, 197–220. [[CrossRef](#)]
- Harrison, H.P. Soil Reactions from Laboratory Studies with an Inclined Blade. *Trans. ASAE* **1982**, *25*, 7–12. [[CrossRef](#)]
- Hettiaratchi, D. Theoretical Soil Mechanics and Implement Design. *Soil Tillage Res.* **1988**, *11*, 325–347. [[CrossRef](#)]
- Reece, A.; Hettiaratchi, D. A Slip-Line Method for Estimating Passive Earth Pressure. *J. Agric. Eng. Res.* **1989**, *42*, 27–41. [[CrossRef](#)]
- Upadhyay, G.; Raheman, H. Comparative analysis of tillage in sandy clay loam soil by free rolling and powered disc harrow. *Eng. Agric. Environ. Food* **2019**, *12*, 118–125. [[CrossRef](#)]
- Nalavade, P.P.; Salokhe, V.M.; Niyamapa, T.; Soni, P. Performance of Free Rolling and Powered Tillage Discs. *Soil Tillage Res.* **2010**, *109*, 87–93. [[CrossRef](#)]
- Mellor, M. *Mechanics of Cutting and Boring. Part 3. Kinematics of Continuous Belt Machines*; Cold Regions Research and Engineering Lab: Hanover, NH, USA, 1976.
- Mellor, M. *Mechanics of Cutting and Boring. Part 8. Dynamics and Energetics of Continuous Belt Machines*; Cold Regions Research and Engineering Lab: Hanover, NH, USA, 1978. Available online: [https://www.arlis.org/docs/vol1/AK\\_Heritage/CRREL/CR/1978/CRREL\\_Rpt-78-11.pdf](https://www.arlis.org/docs/vol1/AK_Heritage/CRREL/CR/1978/CRREL_Rpt-78-11.pdf) (accessed on 18 January 2024).
- Sitorus, P.E.; Ko, J.H.; Kwon, O.S. Parameter study of chain trenching machines of Underwater Construction Robots via analytical model. In Proceedings of the OCEANS 2016 MTS/IEEE Monterey, Monterey, CA, USA, 19–23 September 2016; pp. 1–6.
- Vu, M.T.; Choi, H.; Kim, J.; Tran, N.H. A study on an underwater tracked vehicle with a ladder trencher. *Ocean Eng.* **2016**, *127*, 90–102. [[CrossRef](#)]
- Shmulevich, I.; Asaf, Z.; Rubinstein, D. Interaction Between Soil and a Wide Cutting Blade Using the Discrete Element Method. *Soil Tillage Res.* **2007**, *97*, 37–50. [[CrossRef](#)]

30. Ucgul, M.; Fielke, J.M.; Saunders, C. 3D DEM tillage simulation: Validation of a hysteretic spring (plastic) contact model for a sweep tool operating in a cohesionless soil. *Soil Tillage Res.* **2014**, *144*, 220–227. [[CrossRef](#)]
31. Zeng, Z.; Chen, Y.; Zhang, X. Modelling the Interaction of a Deep Tillage Tool with Heterogeneous soil. *Comput. Electron. Agric.* **2017**, *143*, 130–138. [[CrossRef](#)]
32. Hang, C.; Gao, X.; Yuan, M.; Huang, Y.; Zhu, R. Discrete element simulations and experiments of soil disturbance as affected by the tine spacing of subsoiler. *Biosyst. Eng.* **2018**, *168*, 73–82. [[CrossRef](#)]
33. Hirasawa, K.; Kataoka, T.; Kubo, T. Prediction and Evaluation for Leveling Performance in Rotary Tiller. *IFAC Proc.* **2013**, *46*, 315–320. [[CrossRef](#)]
34. Wang, Y.; Xue, W.; Ma, Y.; Tong, J.; Liu, X.; Sun, J. DEM and soil bin study on a biomimetic disc furrow opener. *Comput. Electron. Agric.* **2019**, *156*, 209–216. [[CrossRef](#)]
35. Zhang, R.; Li, J.; Xu, S.; Li, Y. Simulation on dynamic behavior of dry soil ahead of the bulldozing plate with different cutting angles by DEM. *J. Jilin Univ.* **2007**, *37*, 822–827. (In Chinese) [[CrossRef](#)]
36. Zhang, R.; Chen, B.; Li, J.-Q.; Xu, S.-C. DEM Simulation of Clod Crushing by Bionic Bulldozing Plate. *J. Bionic Eng.* **2008**, *5*, 72–78. [[CrossRef](#)]
37. Ucgul, M.; Saunders, C.; Fielke, J.M. Discrete element modelling of tillage forces and soil movement of a one-third scale mouldboard plough. *Biosyst. Eng.* **2017**, *155*, 44–54. [[CrossRef](#)]
38. Ucgul, M.; Saunders, C. Simulation of tillage forces and furrow profile during soil-mouldboard plough interaction using discrete element modelling. *Biosyst. Eng.* **2020**, *190*, 58–70. [[CrossRef](#)]
39. Tong, J.; Jiang, X.-H.; Wang, Y.-M.; Ma, Y.-H.; Li, J.-W.; Sun, J.-Y. Tillage Force and Disturbance Characteristics of Different Geometric-Shaped Subsoilers Via DEM. *Adv. Manuf.* **2020**, *8*, 392–404. [[CrossRef](#)]
40. Wang, X.; Li, P.; He, J.; Wei, W.; Huang, Y. Discrete Element Simulations and Experiments of Soil-Winged Subsoiler Interaction. *Int. J. Agric. Biol. Eng.* **2021**, *14*, 50–62. [[CrossRef](#)]
41. Hettiaratchi, D. The Present State of the Theory of Soil Cutting. *J. Terramechanics* **1965**, *2*, 63–76. [[CrossRef](#)]
42. Salokhe, V.; Pathak, B. Effect of Aspect Ratio on Soil Failure Pattern Generated by Vertical Flat Tines at Low Strain Rates in Dry Sand. *J. Agric. Eng. Res.* **1992**, *53*, 169–180. [[CrossRef](#)]
43. Hang, C.; Gao, X.; Wang, B.; Yuan, M.; Huang, Y.; Zhu, R. Optimization of the Wing Parameters for a Winged Subsoiler. *Appl. Eng. Agric.* **2017**, *33*, 313–319. [[CrossRef](#)]
44. McKyes, E.; Maswaure, J. Effect of design parameters of flat tillage tools on loosening of a clay soil. *Soil Tillage Res.* **1997**, *43*, 195–204. [[CrossRef](#)]
45. Hang, C.; Yao, Y.; Huang, Y.; Li, W.; Zhu, R. High-Speed Photographic Analysis of the Soil Disturbance Affected by Subsoiler Rake Angle. *Agric. Eng. Int. CIGR J.* **2017**, *19*, 42–50.
46. McKyes, E.; Ali, O. The cutting of soil by narrow blades. *J. Terramechanics* **1977**, *14*, 43–58. [[CrossRef](#)]
47. Coetzee, C.J. The Modelling of Granular Flow Using the Particle-in-Cell Method. Ph.D. Thesis, University of Stellenbosch, Stellenbosch, South Africa, April 2004. Available online: <https://scholar.sun.ac.za/handle/10019.1/1334> (accessed on 18 January 2024).
48. Mouazen, A.M.; Neményi, M. Tillage tool design by the finite element method: Part 1. finite element modelling of soil plastic behaviour. *J. Agric. Eng. Res.* **1999**, *72*, 37–51. [[CrossRef](#)]
49. Chi, L.; Kushwaha, R. A non-linear 3-D finite element analysis of soil failure with tillage tools. *J. Terramechanics* **1990**, *27*, 343–366. [[CrossRef](#)]
50. Hryciw, R.D.; Raschke, S.A.; Ghalib, A.M.; Horner, D.A.; Peters, J.F. Video tracking for experimental validation of discrete element simulations of large discontinuous deformations. *Comput. Geotech.* **1997**, *21*, 235–253. [[CrossRef](#)]
51. Karmakar, S.; Kushwaha, R.L.; Stilling, D.S.D. Propagation of Soil Failure Front Associated with various Agricultural Tillage Tools. In Proceedings of the 2003 ASAE Annual Meeting, Las Vegas, NV, USA, 27–30 July 2003.
52. Sharifat, K.; Kushwaha, R.L. Modeling Soil Movement by Tillage Tools. *Can. Agric. Eng.* **2000**, *42*, 165–172. Available online: [https://library.csbe-scgab.ca/docs/journal/42/42\\_4\\_165\\_ocr.pdf](https://library.csbe-scgab.ca/docs/journal/42/42_4_165_ocr.pdf) (accessed on 18 January 2024).
53. Hettiaratchi, D. A Critical State Soil Mechanics Model for Agricultural Soils. *Soil Use Manag.* **1987**, *3*, 94–105. [[CrossRef](#)]
54. Hettiaratchi, D. The Development of a Powered Low Draught Tine Cultivator. *Soil Tillage Res.* **1993**, *28*, 159–177. [[CrossRef](#)]
55. Spoor, G.; Fry, R. Soil Disturbance Generated by Deep-Working Low Rake Angle Narrow Tines. *J. Agric. Eng. Res.* **1983**, *28*, 217–234. [[CrossRef](#)]
56. Reece, A.R. SOIL Mechanics of agricultural soils. *Soil Sci.* **1977**, *123*, 332–337. [[CrossRef](#)]

**Disclaimer/Publisher’s Note:** The statements, opinions and data contained in all publications are solely those of the individual author(s) and contributor(s) and not of MDPI and/or the editor(s). MDPI and/or the editor(s) disclaim responsibility for any injury to people or property resulting from any ideas, methods, instructions or products referred to in the content.